Real-time near-field acoustic holography for continuously visualizing nonstationary acoustic fields

J.-H. Thomas,[a] V. Grulier, S. Paillasseur, and J.-C. Pascal
Laboratoire d'Acoustique de l'Université du Maine (Unité Mixte de Recherche-CNRS 6613), Avenue O. Messiaen, 72085 Le Mans Cedex 09, France

J.-C. Le Roux
Centre de Transfert de Technologie du Mans, 20 rue Thales de Milet, 72000 Le Mans, France

(Received 21 December 2009; revised 17 September 2010; accepted 23 September 2010)

Near-field acoustic holography (NAH) is an effective tool for visualizing acoustic sources from pressure measurements made in the near-field of sources using a microphone array. The method involving the Fourier transform and some processing in the frequency-wavenumber domain is suitable for the study of stationary acoustic sources, providing an image of the spatial acoustic field for one frequency. When the behavior of acoustic sources fluctuates in time, NAH may not be used. Unlike time domain holography or transient method, the method proposed in the paper needs no transformation in the frequency domain or any assumption about local stationary properties. It is based on a time formulation of forward sound prediction or backward sound radiation in the time-wavenumber domain. The propagation is described by an analytic impulse response used to define a digital filter. The implementation of one filter in forward propagation and its inverse to recover the acoustic field on the source plane implies by simulations that real-time NAH is viable. Since a numerical filter is used rather than a Fourier transform of the time-signal, the emission on a point of the source may be rebuilt continuously and used for other post-processing applications.
 [DOI: 10.1121/1.3504656]

PACS number(s): 43.60.Sx, 43.60.Pt, 43.60.Gk [EJS] Pages: 3554–3567

I. INTRODUCTION

Near-field acoustic holography (NAH) is a well-known technique for recovering the sound field of an acoustic system when the signals emitted by the sources are stationary. It makes it possible to visualize the spatial pressure field radiated by the system for any frequency of interest. The principle of the method in the case of planar NAH entails first acquiring the pressure field from a square area in the near-field of the system studied using a microphone array. Then a specialized processing technique in the wavenumber domain is used to back-propagate the pressure field from z_A to z_s as shown in Fig. 1. This technique, described in depth in Ref. 1, involves amplifying the evanescent waves measured in the near-field. But this may cause erroneous values in the reconstructed pressure field, particularly because of the presence of measurement noise. Fortunately the ill-posed back-propagation inverse problem may be solved by several methods such as exponential,[1] Wiener,[2,3] or adaptative[4] filtering in the wavenumber domain or Tikhonov regularization.[5] It is also possible and easier, from the knowledge of the measurement pressure field in z_A, to predict the forward pressure field in z_F (see Fig. 1). This problem is referred to as direct problem.

However, monitoring a system in order to detect any defects or predict the presence of inappropriate conditions requires inspection of the time evolution of some features designed to highlight the behavior of the system. It is particularly true for acoustic systems which radiate nonstationary sounds. When the statistical properties of the emitted acoustic signals fluctuate in time, standard NAH is unsuitable because the spatial pressure field obtained by the method fluctuates in time. Several authors have presented some developments to standard NAH to take into account the nonstationary properties of the studied acoustic signals.[6–9] The differences between the methods presented in these works and the technique proposed in the paper will be discussed further. We can simply say now that they use standard NAH to process one, several, or all frequencies before coming back to the time domain. Another study concerns the reconstruction of transient acoustic quantities by means of the Helmholtz equation least squares method.[10] Even if the approach is based on a convolution over time kernels, its principle differs largely from the other derived NAH methods referred to insofar as a spherical source assumption is made. An approach for source reconstruction in the time domain has also been proposed,[11] based on the inversion method of transfer functions, studied by Nelson and Yoon,[12] between the mesh on the source plane and the microphone array. Bai and Lin use the regularized solutions of the inverse problem for each frequency to construct a digital filter bank.[11]

As our objective is also to deal with time-evolving acoustic fields, we propose to start with the formulation which provides, in the time-wavenumber domain, a time-evolving acoustic field in a forward plane by applying a convolution between the instantaneous wavenumber spectrum and an impulse response.[13,14] The issue is then to invert the impulse response in order to apply a similar formulation that involves in the same domain, a convolution between the measured

[a]Author to whom correspondence should be addressed. Electronic mail: jean-hugh.thomas@univ-lemans.fr

 0001-4966/2010/128(6)/3554/14/$25.00

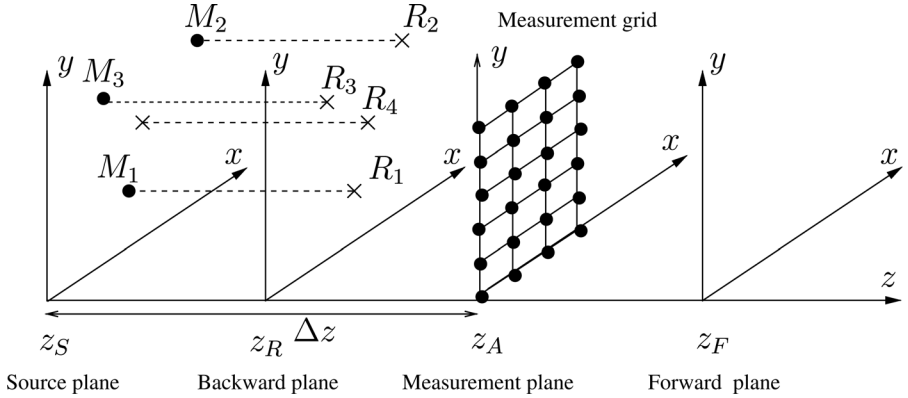

FIG. 1. Geometry: For the inverse problem, the sound field in the source plane $z = z_S$ has to be back-propagated from the sound field acquired in $z = z_A$. For the direct problem, the sound field in the forward plane $z = z_F$ has to be predicted from the sound field acquired in $z = z_A$. The numerical study involves three nonstationary monopole sources M_1, M_2, and M_3. The aim is to reconstruct the sound field in the plane $z = z_R$.

instantaneous wavenumber spectrum and the inverse impulse response. Thus this processing allows one to continuously reconstruct the acoustic field on the source plane as if there were a microphone array directly integrated into the sources. The aim of this paper is to present the so-called real-time near-field acoustic holography (RT-NAH) method, to compare it with other methods dealing with the visualization of time-evolving acoustic fields and to highlight its characteristics. First, the term "real-time" is not chosen to describe a hardware configuration with multiprocessing but to underline the fact that the acoustic field reconstruction is continuously done in time. Even if many papers deal with standard NAH, Sec. II describes NAH in order to make the reader better understand the similarities and the differences between the methods discussed in the paper. Section III is dedicated to other methods in the literature, which are interested in visualizing transient acoustic signals. These methods are categorized according to the information provided. Then RT-NAH method is presented in Sec. IV. After a description of the theory, an interpretation is given in the frequency domain. It is particularly shown how the method takes into account both propagating and evanescent waves even though the two types of wave cannot be separated in the wavenumber domain as for standard NAH. Section IV ends with the inversion of the impulse response in the time-wavenumber domain, which is the heart of the problem. Several preprocessed impulse responses in accordance with Ref. 14 are inverted using optimum filtering. The feasibility of the method is tested in simulation with three monopole sources driven by nonstationary signals without noise or regularization processing. Results are discussed in Sec. V from objective indicator values, reconstructed time-signals, and spatial acoustic field maps.

II. NAH FOR STATIONARY ACOUSTIC SOURCES

NAH is implemented using both one and two dimensional discrete Fourier transforms (see Fig. 2). The acquisition of acoustic signals from the measurement surface gives a time-space representation of the pressure noted $p(x, y, z_A, t)$. Because of the stationary characteristic of the sources, the pressure field is acquired at different moments, from the displacement of a single microphone or a small microphone array using a two-axis robot. Then, the phase relationships between the pressure measurements are recovered from a pressure signal acquired from a fixed-location reference microphone. The cross-spectrum $S_{RP}(\omega)$ between each spatial pressure measurement $p(x, y, z_A, t)$ and the reference signal, and the autospectrum $S_R(\omega)$ of the reference, combined as shown in Eq. (1), yield the frequency-dependent spatial pressure field $p(x, y, z_A, \omega)$,

$$P(x, y, z_A, \omega) = \frac{S_{RP}(\omega)}{\sqrt{S_R(\omega)}}. \tag{1}$$

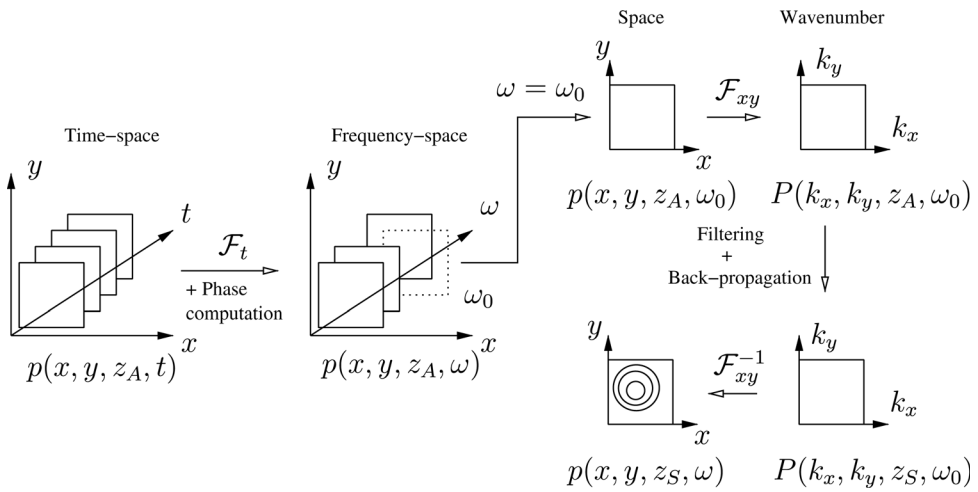

FIG. 2. Synopsis of NAH processing for stationary sources. According to Eq. (1), the phase computation involves Fourier transforms of time-signals ($\mathcal{F}_t$ operator). $\mathcal{F}_{x,y}$ and $\mathcal{F}_{x,y}^{-1}$ operators imply direct and inverse spatial two dimensional Fourier transforms.

When the sound field is generated by a composite source comprising mutually incoherent sources, it is necessary to use several references. A multireference procedure based on singular value decomposition and described in terms of a reference cross-spectral matrix and a cross-spectral matrix linking the reference and measured signals can be used to separate the total sound field into a set of partial fields that are incoherent with each other.[15–17] It is usual to then extract the spatial pressure field $p(x, y, z_A, \omega_0)$ from the measurement surface for a chosen angular frequency ω_0 or for several frequencies of a frequency band. In order to choose these frequencies, the whole pressure radiated by the system is computed, which makes the most important frequencies emerge.

The aim of NAH is now to obtain the spatial pressure field $p(x, y, z_S, \omega_0)$ for ω_0 on the source plane. This is done in the frequency-wavenumber domain using $\mathcal{R}$ operator in charge of back-propagation and regularization. The purpose here is not to give a detailed description of the techniques of regularization, which are, in particular, reported in Ref. 5. The transformation to the wavenumber domain is provided by $\mathcal{F}_{x,y}$ operator representing the two dimensional spatial Fourier transform. The use of inverse operator $\mathcal{F}_{x,y}^{-1}$ is necessary, as mentioned in Fig. 2 and Eq. (2), to obtain $p(x, y, z_S, \omega_0)$, the spatial pressure field of the system studied for angular frequency ω_0,

$$p(x, y, z_s, \omega_0) = \mathcal{F}_{x,y}^{-1} \mathcal{R}\, \mathcal{F}_{x,y}\, p(x, y, z_A, \omega_0), \tag{2}$$

with the following definitions of operators $\mathcal{F}_{x,y}$ and $\mathcal{F}_{x,y}^{-1}$:

$$\mathcal{F}_{x,y} \equiv \int_{-\infty}^{+\infty} \int_{-\infty}^{+\infty} e^{jk_x x} e^{jk_y y} dxdy, \tag{3}$$

$$\mathcal{F}_{x,y}^{-1} \equiv \left(\frac{1}{2\pi}\right)^2 \int_{-\infty}^{+\infty} \int_{-\infty}^{+\infty} e^{-jk_x x} e^{-jk_y y} dk_x dk_y. \tag{4}$$

Therefore, the great advantage of NAH is to provide an image of the spatial pressure field for one frequency or a frequency band that allows one to locate the parts of the system studied which radiate the most. In addition to pressure, NAH also provides other features like velocity and acoustic intensity. Furthermore, when dealing with stationary acoustic sources, NAH is inexpensive in terms of experimental devices. Indeed, it is not necessary to have as many acquisition channels as the total number of measurement points on the hologram plane. As previously indicated, a relatively small number of scan microphones may be used in combination with reference microphones. The scanning method using a moving frame technique with a microphone line array which travels over the measurement plane at a constant speed is also a low cost alternative.[18]

III. NAH FOR NONSTATIONARY ACOUSTIC SOURCES

The approaches[6–9] used to backward project transient nonstationary sound pressure fields come from the same theory. The starting point is the wave-equation in Cartesian geometry

$$\nabla^2 p(x, y, z, t) - \frac{1}{c^2} \frac{\partial^2 p(x, y, z, t)}{\partial t^2} = 0, \tag{5}$$

(where c denotes the sound speed) on which a three-dimension Fourier transform, with respect to space and time, is operated, yielding the expression

$$P(k_x, k_y, z, \omega) = \int_{-\infty}^{+\infty} \int_{-\infty}^{+\infty} \int_{-\infty}^{+\infty} p(x, y, z, t)\, e^{-j\omega t} \times e^{j(k_x x + k_y y)} dt\, dk_x\, dk_y \tag{6}$$

of the pressure $P(k_x, k_y, z, \omega)$ in the frequency-wavenumber domain.

These methods fall into two categories according to the information provided. The first idea leads to obtain time-signals on each node of the mesh on the source plane that is the image of the measurement surface.[6–8] It is as if the time measurements had been made directly on the surface including the acoustic sources. The second idea involves providing, for a chosen frequency band, a time-dependent map of the spatial pressure field on the source plane which is, on the whole, a logical continuation of standard NAH dedicated to stationary sources.[9] The common point of these methods is, except for repeatable sources, the simultaneous acquisition of the pressure signals from the measurement grid. The method proposed in the paper belongs to the first category in terms of information provided.

A. Time-dependent pressure

Hald proposed to reconstruct the pressure time-signals on the source plane from signals acquired by a microphone array.[6–8] The starting point of the method, called "time domain method" which is particularly well-adapted to the study of short time events, is the acquisition of acoustic time-signals. However, long time sequences can be recorded, and in this case, time intervals have to be selected for processing. Let us describe the operations on one block of time data of T seconds. The Fourier transform computed on the time-dependent pressure signal acquired from each point of the measurement area, as for standard NAH (see Fig. 3), gives a set of spectra for each measurement point. Then the spatial pressure fields $p(x, y, z_A, \omega)$, on the plane at a distance $z_A - z_S$ from the source plane, are extracted for each angular frequency ω. The two dimensional Fourier transforms are applied, yielding the values $P(k_x, k_y, z_A, \omega)$ in the wavenumber domain for each ω also. After that, the back-propagation operator is applied to each spectral line yielding the wavenumber spectrum $P(k_x, k_y, z_S, \omega)$ on the source plane. The computation with the inverse two dimensional Fourier transform provides the frequency-spatial pressure field $p(x, y, z_S, \omega)$ on the source plane. Then, a point (x_0, y_0) of the spatial grid is chosen giving the frequency-dependent pressure $p(x_0, y_0, z_S, \omega)$. Finally, an inverse Fourier transform allows the reconstruction of the time-dependent pressure $p(x_0, y_0, z_S, t)$ for the specified space location on the source plane. The following equation sums up the time domain method,

$$p(x, y, z_S, t) = \mathcal{F}_t^{-1} \mathcal{F}_{x,y}^{-1} \mathcal{R}\, \mathcal{F}_{x,y}\, \mathcal{F}_t\, p(x, y, z_A, t). \tag{7}$$

Deblauwe *et al.* used also this method in order to study an acoustic short time event of less than a second like a nonrepeatable impact noise.[9] A derivation of this method has been proposed and tested recently in order to study the sound

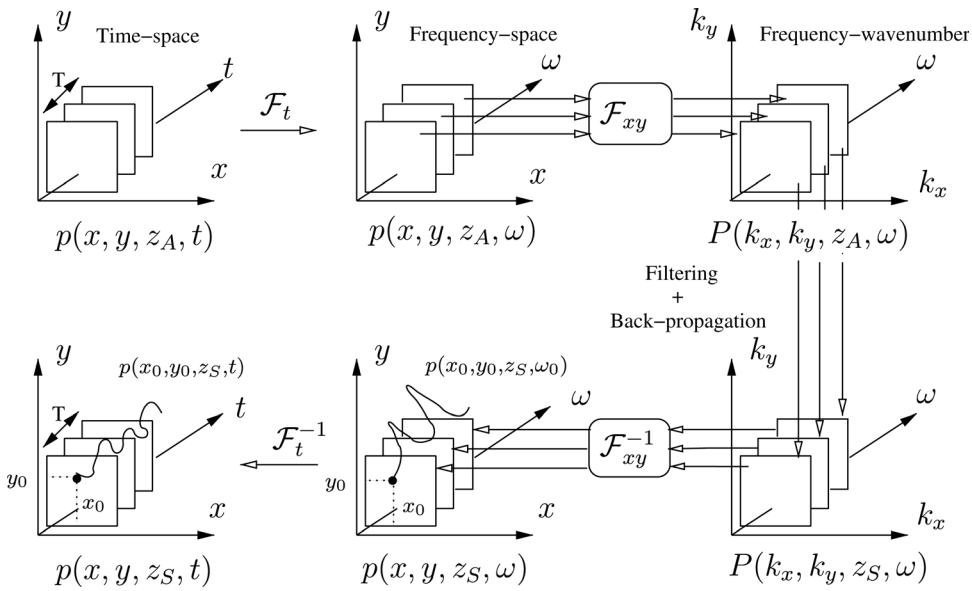

FIG. 3. Synopsis of time domain holography for nonstationary sources highlighting time-dependent acoustic pressure on the source plane.

pressure radiated by a free Plexiglas plate impacted by a steel pendulum.[19] The Fourier operators with respect to time $\mathcal{F}_t$ and $\mathcal{F}_t^{-1}$ are then replaced with Laplace operators. This change would suppress aliasing errors but requires a regularization process to limit the instabilities due to the inversion of the numerical Laplace transform.

The time domain method should preferably be applied, using Fourier or Laplace operators, to one pressure time-signal of finite duration only. Therefore, the nonstationary studied event must be short. Indeed, in the time domain method, standard NAH has to be reiterated as many times as there are spectral lines. And the whole process has to be reiterated if several data blocks are considered with long time sequences. In addition, the possible use of a regularization technique (L curve or generalized cross-validation)[20] to reconstruct the source plane at each frequency becomes enormously time-consuming. An exponential or Wiener filtering in the wavenumber domain seems then more suitable. All the microphone signals should be acquired at the same time.

However, the technique may be used on repeatable nonstationary signals. It was done in the more simple case of forward (not backward) prediction of sound pressure fields by La Rochefoucauld *et al.*[21] A 4×4 square array moved by a two-axis robot is then used to acquire the pressure field radiated by two loudspeakers and a baffled plate on a 8×8 or a 28×20 grid of measurement points. The goal is then to reconstruct, during a short period of about 5 ms, the time pressure signals on a plane $z = z_F$ from the signals recorded on the plane $z = z_A$ (see Fig. 1). Accurate results are obtained when the propagation distance $z_F - z_A$ is small compared with the wavelength λ_{mean} calculated from the frequency of the spectrum maximum $[(z_F - z_A)/\lambda_{\text{mean}} \leq 0.35]$. Note that this direct problem has also been investigated when the time domain method is implemented using numerical Laplace transforms.[22]

B. Time-dependent spatial pressure field for one frequency

Deblauwe *et al.*'s work focuses on a time-evolving spatial map of the pressure field.[9] The aim of the study is to provide $p(x, y, z_S, \tau, \omega_0)$, the time-dependent pressure field radiated by an acoustic system directly on the plane source, into a time interval centered at time $t = \tau$, for a specific frequency ω_0. The major development of this method called "transient method" is the use of a short time Fourier transform (STFT) on the acoustic time-signals acquired by the microphone array (see Fig. 4). For each angular frequency ω, this operation provides the time-dependent spatial pressure field $p(x, y, z_A, \tau, \omega)$ on the plane at a distance z_A from the source plane. Then, once a frequency ω_0 has been chosen, the NAH processing technique described in Sec. II is iterated, for the frequency studied ω_0, on the spatial pressure field $p(x, y, z_A, \tau, \omega_0)$, for each time interval τ. The method ends with the recovered time-evolving spatial pressure field $p(x, y, z_S, \tau, \omega_0)$ on the source plane. Equations (8) and (9) formalize the method

$$p(x, y, z_S, \tau, \omega_0) = \mathcal{F}_{x,y}^{-1} \mathcal{R} \, \mathcal{F}_{x,y} \, p(x, y, z_A, \tau, \omega_0) \tag{8}$$

with

$$\begin{aligned} p(x, y, z_A, \tau, \omega_0) &= p(x, y, z_A, \tau, \omega)|_{\omega=\omega_0}, \\ &= \mathcal{F}_t \, p(x, y, z_A, t) \theta(t - \tau)|_{\omega=\omega_0}, \end{aligned} \tag{9}$$

where $\theta(t)$ denotes the window used for the pieces of the signal and $\mathcal{F}_t$, the following Fourier operator

$$\mathcal{F}_t \equiv \int_{-\infty}^{+\infty} e^{-j\omega t} dt. \tag{10}$$

The main advantage of this approach is that there is no limitation on the length of the acoustic time-signals studied because the processing method operates on pieces of time-signals. This is due to the use of the windowed Fourier transform. The resolution in time and frequency depends on the spread of the window used for the STFT. It is well established that the two resolutions are dependent due to the Heisenberg uncertainty principle.[23] The spread of the window must be set once and for all. Hence the time and frequency resolutions are stated. The disadvantage of this approach comes from this

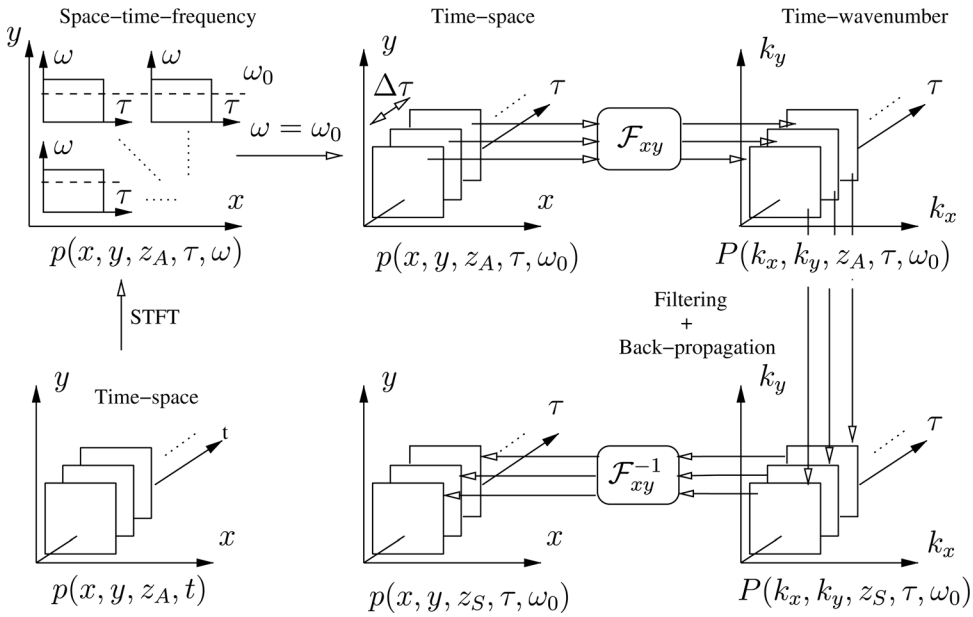

FIG. 4. Synopsis of the transient method for nonstationary sources, highlighting, for a given frequency ω_0, the time-dependent spatial pressure field on the source plane (STFT).

point. Since the acoustic system studied is not stationary, different patterns may occur such as fast transient signals and signals with slower variations. In this case, the spread of the window chosen for the analysis may be suitable for one pattern but not for the other. It is known in speech analysis that a window suitable for the analysis of vowels is not so for consonants. When the spread of the window is large, increasing the frequency resolution, the resolution in time decreases even if the pieces of the signal are made to overlap significantly. Let us consider the maximum overlap of pieces leading to a spatial pressure field mapping every $\Delta\tau = 1/f_e$, where f_e denotes the sampling frequency. If a short transient signal appears, traces of the pattern would be noticed on the representations for several moments whose duration overruns that of the phenomenon itself.

For this method, which provides a time-dependent spatial pressure field for one frequency, acquisitions from the points of the measurement area need to be processed at the same time which implies a system of about 100 channels. However, for specific engine applications involving relatively slow run-ups such as a revolution increment per minute of 250, per second or less, Deblauwe *et al.* claim that in practice the phase relationship between points of the measurement area is repeatable according to different runs.[9] In this specific way, the analysis, where the time axis is replaced by a rpm (revolutions per minute) axis, can be done without the need of a high channel count acquisition system.

IV. RT-NAH

A. Theory

A formulation for radiating acoustic sources given in the time-wavenumber domain was proposed by Forbes *et al.*[13] This formulation has the advantage to allow one to continuously reconstruct the pressure field at a plane $z = z_F$ from measurements done in a plane $z = z_A$ with the configuration shown in Fig. 1. In a recent study the approach was revisited, its accuracy was discussed, and the results obtained on simulated cases implementing the direct problem encouraged us to investigate the inverse problem.[14]

The direct problem is described by means of a convolution product in the time-wavenumber domain between the time-dependent wavenumber spectrum $P(k_x, k_y, z_A, t)$ and an impulse response $h(k_x, k_y, z_F - z_A, t)$,

$$P\left(k_x, k_y, z_F, t\right) = P\left(k_x, k_y, z_A, t\right) * h\left(k_x, k_y, z_F - z_A, t\right). \tag{11}$$

The forward radiation can also be considered from the source plane $z = z_S$ to the measurement plane $z = z_A$. Then,

$$P\left(k_x, k_y, z_A, t\right) = P\left(k_x, k_y, z_S, t\right) * h\left(k_x, k_y, z_A - z_S, t\right). \tag{12}$$

According to Ref. 14, the impulse response $h(k_x, k_y, z_A - z_S, t)$ can be written using the notations for the propagation distance $\Delta z = z_A - z_S$, the wavenumber $k_r = \sqrt{k_x^2 + k_y^2}$, the propagation delay $\tau = \Delta z/c$, and the transition pulsation $\Omega_r = ck_r$,

$$\begin{aligned} h\left(k_x, k_y, z_A - z_S, t\right) &= h(\Omega_r, \tau, t) \\ &= \delta(t - \tau) - g(\Omega_r, \tau, t), \end{aligned} \tag{13}$$

with $\delta(t)$ as the Dirac delta function and where

$$g(\Omega_r, \tau, t) = \tau\,\Omega_r^2 \frac{J_1\left(\Omega_r\sqrt{t^2 - \tau^2}\right)}{\Omega_r\sqrt{t^2 - \tau^2}}\Gamma(t - \tau). \tag{14}$$

J_1 denotes the first order Bessel function of the first kind and $\Gamma(t)$, the Heaviside step function defined by

$$\Gamma(t) = \begin{cases} 0 & \text{for } t < 0, \\ \frac{1}{2} & \text{for } t = 0, \\ 1 & \text{for } t > 0. \end{cases} \tag{15}$$

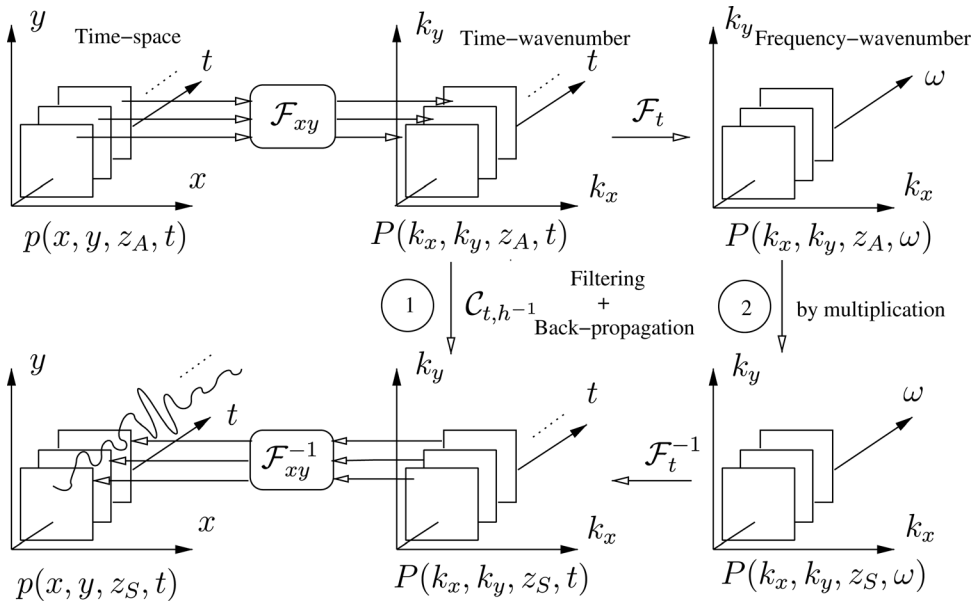

FIG. 5. Synopsis of RT-NAH processing for nonstationary sources highlighting time-dependent acoustic pressure on the source plane [path (1)]. The configuration with path (2) depicts Eq. (18).

The approach called RT-NAH has the ability to continuously reconstruct the time-dependent acoustic signals located in a virtual grid facing the microphone array. It has the same theoretical basis as the two previously discussed methods, but it does not require to work in the frequency domain to reconstruct the acoustic field on the source plane, including the evanescent waves. The RT-NAH method reaches this goal by performing the inverse operation of that described by Eq. (12),

$$P(k_x,k_y,z_S,t) = P(k_x,k_y,z_A,t) * h^{-1}(k_x,k_y,\Delta z,t), \quad (16)$$

where $h^{-1}(k_x,k_y,\Delta z,t)$ is an inverse impulse response operating in the time-wavenumber domain to back-propagate the pressure field from the measurement plane to the source plane. The objective here is to provide the time-dependent pressure signal on the source plane as for the time-method by computing $h^{-1}(k_x,k_y,\Delta z,t)$. The synopsis of the method is described in Fig. 5. Using operator $\mathcal{C}_{t,h^{-1}}$ of time convolution over the inverse impulse response $h^{-1}(k_x,k_y,\Delta z,t)$, RT-NAH may be described by the following equation:

$$p(x,y,z_S,t) = \mathcal{F}_{x,y}^{-1}\mathcal{C}_{t,h^{-1}}\mathcal{F}_{x,y}\,p(x,y,z_A,t). \quad (17)$$

B. Interpretation in the frequency domain

Considering that Fourier operators are commutative, Eq. (7) giving the time-dependent spatial pressure field on the source plane may be re-written as

$$p(x,y,z_S,t) = \mathcal{F}_{x,y}^{-1}\mathcal{F}_t^{-1}\mathcal{R}\,\mathcal{F}_t\mathcal{F}_{x,y}\,p(x,y,z_A,t). \quad (18)$$

The step which provides the pressure field $P(k_x,k_y,z_S,t)$ on the source plane in a time-wavenumber domain from that on the measurement plane in the same domain is

$$P(k_x,k_y,z_S,t) = \mathcal{F}_t^{-1}\mathcal{R}\mathcal{F}_t\,P(k_x,k_y,z_A,t). \quad (19)$$

Equation (19) is re-written with the unique operator $\mathcal{C}_{t,h^{-1}}$ of Eq. (17) corresponding to the time convolution as

$$P(k_x,k_y,z_S,t) = \mathcal{C}_{t,h^{-1}}P(k_x,k_y,z_A,t). \quad (20)$$

It is noticeable that the Fourier transform of Eq. (12) with respect to time yields

$$P(k_x,k_y,z_A,\omega) = P(k_x,k_y,z_S,\omega)\,H(\Omega_r,\tau,\omega), \quad (21)$$

where $H(\Omega_r,\tau,\omega)$ is the frequency response of the acoustic radiation. $H(\Omega_r,\tau,\omega)$ is well known in NAH[1] since it is defined as the propagator from the plane $z = z_S$ to the plane $z = z_A$ such as

$$H(\Omega_r,\tau,\omega) = \begin{cases} e^{-j\tau\sqrt{\omega^2-\Omega_r^2}} & \text{for } \omega \geq \Omega_r, \\ e^{-\tau\sqrt{\Omega_r^2-\omega^2}} & \text{for } \omega < \Omega_r. \end{cases} \quad (22)$$

This propagator is usually represented at a given frequency as a function of wavenumber ($k_r = \sqrt{k_x^2+k_y^2}$), whereas the idea here is to express it for a given wavenumber ($k_r = \Omega_r/c$) as a function of angular frequency. The inverse problem can be analyzed in the frequency domain by directly inverting the frequency response $H(\Omega_r,\tau,\omega)$ in Eq. (22), yielding the inverse frequency response

$$H^{-1}(\Omega_r,\tau,\omega) = \frac{1}{H(\Omega_r,\tau,\omega)} = \begin{cases} e^{j\tau\sqrt{\omega^2-\Omega_r^2}} & \text{for } \omega \geq \Omega_r, \\ e^{\tau\sqrt{\Omega_r^2-\omega^2}} & \text{for } \omega < \Omega_r. \end{cases} \quad (23)$$

$H^{-1}(\Omega_r,\tau,\omega)$ allows one to obtain the time-wavenumber pressure $P(k_x,k_y,z_S,t)$ on the source plane $z = z_S$ from the time-wavenumber pressure $P(k_x,k_y,z_A,t)$ on the measurement plane $z = z_A$ according to Eq. (24) which is also the Fourier transform of Eq. (16),

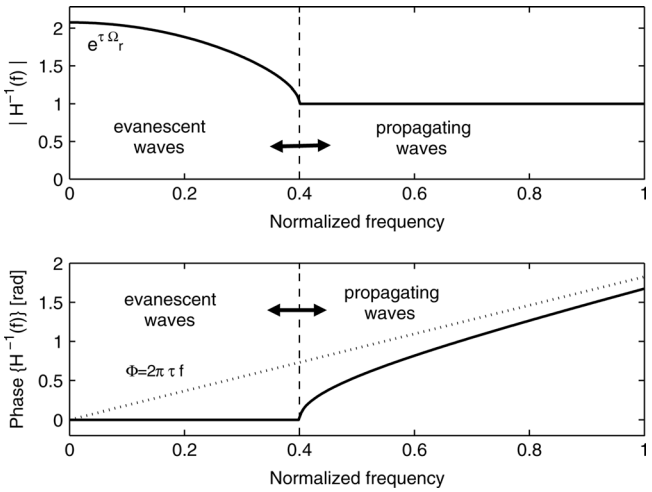

FIG. 6. Magnitude and phase in rad of the theoretical inverse transfer function $H^{-1}(\Omega_r,\tau,f)$ for the normalized transition frequency $f_r/(f_e/2)=0.4$ and the propagation distance $\Delta z=0.05$ m.

$$P\left(k_x,k_y,z_S,\omega\right)=P\left(k_x,k_y,z_A,\omega\right)H^{-1}(\Omega_r,\tau,\omega). \quad (24)$$

The modulus and the phase of the inverse frequency response $H^{-1}(\Omega_r,\tau,\omega)$ are shown in Fig. 6. In the case of RT-NAH, as for the direct problem described in Ref. 14, the transition frequency $f_r=\Omega_r/2\pi$ takes an important part. It separates two kinds of wave behavior in the frequency-wavenumber domain. The components of the time-evolving wavenumber spectrum $P(k_x,k_y,z_A,t)$ with a frequency $f\geq f_r$ behave as propagating waves. Their back-propagation leads to a change of phase, but their amplitudes remain unchanged. The components $P(k_x,k_y,z_A,t)$ with a frequency $f<f_r$ behave as evanescent waves. Their back-propagation leads to an amplification of their amplitudes, but their phases remain unchanged. This amplification may induce erroneous values in the presence of measurement noise and thus is a difficult point for solving the inverse problem. The value of the normalized transition frequency for a transfer function associated with a wavenumber (k_x,k_y) also indicates the proportion of evanescent waves processed. The latter will obviously result in difficulties in the inverse process. The influence of the transition frequency highlights the specificity of RT-NAH method dedicated to fluctuating sources. In RT-NAH, processing in the time-wavenumber domain does not lead to separate propagating and evanescent waves while both kinds of wave are well separated in the wavenumber domain in standard holography. However, as reported before, propagating and evanescent wave components are differently processed by $h^{-1}(k_x,k_y,\Delta z,t)$ in RT-NAH. Since the goal of the study is to compute the inverse impulse response $h^{-1}(k_x,k_y,\Delta z,t)$, the current discussion gives an evident solution. By sampling in the frequency domain the analytic inverse transfer function $H^{-1}(\Omega_r,\tau,\omega)$ in Eq. (23) and then by operating the inverse Fourier transform, the time-wavenumber inverse impulse response is obtained. This method is denoted Fourier-I (FI).

Another approach is to start with an expression of the impulse response $h(k_x,k_y,\Delta z,t)$ describing the direct problem [see Eq. (12)] and then to invert it. It is clear that having the analytic expression of $g(k_x,k_y,\Delta z,t)$ [Eq. (14)] which is linked to $h(k_x,k_y,\Delta z,t)$ by Eq. (13) seems comforting. However, Grulier, who investigated various pre-processed impulse responses,[24] demonstrated that it is necessary to carefully sample $g(k_x,k_y,\Delta z,t)$. According to a numerical work involving monopole sources driven by nonstationary signals,[14] three methods can be chosen to implement the impulse response rather than directly sample it. These methods used to provide operational impulse responses for the inversion process are briefly introduced in Sec. IV C. Another technique tested here to provide the discretized impulse response $h(k_x,k_y,\Delta z,t)$ consists of directly operating the inverse discrete Fourier transform on the analytical transfer function $H(\Omega_r,\tau,\omega)$ in Eq. (22). The approach is called Fourier-D (FD) method.

Before defining the inverse impulse response $h^{-1}(k_x,k_y,\Delta z,t)$, let us give the expression of the impulse response used $h(k_x,k_y,\Delta z,t)$.

C. Processing the direct impulse response

The four treatments applied to the theoretical function $g(\Omega_r,\tau,t)$ in Eq. (14), detailed in Refs. 14 and 24, are summarized as follows:

(1) *Direct method:* $g(\Omega_r,\tau,t)$ is sampled at discrete equidistant instants in time.
(2) *Average method:* $g(\Omega_r,\tau,t)$ is average sampled. For each time $t=n\tau$, the mean value $\bar{g}(\Omega_r,\tau,t)$ is computed into the interval Δt centered at $t=n\tau$ using an integral.
(3) *Chebyshev method:* $g(\Omega_r,\tau,t)$ is low-pass filtered using a Chebyshev filter with a cutoff frequency $f_c=6400$ Hz. It is achieved by upsampling $g(\Omega_r,\tau,t)$ by the factor $D=8$, using the low-pass filter and then downsampling the resulting response by the factor $1/D$.
(4) *Numerical Kaiser method:* $g(\Omega_r,\tau,t)$ is low-pass filtered using a Kaiser-Bessel filter with a cutoff frequency $f_c=6640$ Hz. An upsampling factor of $D=2$ is used, and the integral for the convolution is numerically computed using the trapezoidal method.

D. Inverting the impulse response

Suppose that a processing method among those described before is used to provide N samples of $g(\Omega_r,\tau,n)$. The impulse response $h(\Omega_r,\tau,n)$ or $h(k_x,k_y,\Delta z,n)$ describing the acoustic radiation from the source plane $z=z_S$ to the measurement plane $z=z_A$ is deduced from Eq. (13). The goal of this step is now to find out the inverse filter with the impulse response $h^{-1}(k_x,k_y,\Delta z,n)$ that recovers the discrete time-dependent wavenumber spectrum $P(k_x,k_y,z_S,n)$ on the source plane, according to the discretized version of Eq. (16),

$$P\left(k_x,k_y,z_S,n\right)=P\left(k_x,k_y,z_A,n\right)*h^{-1}\left(k_x,k_y,\Delta z,n\right). \quad (25)$$

The number of coefficients N of the direct causal filter with a finite-duration impulse response (FIR) is chosen, supposing that after a duration of $N\times T_e$ seconds (T_e is the inverse of the sampling frequency), the oscillations of the impulse response are very weak and then insignificant. To provide the inverse impulse response $h^{-1}(k_x,k_y,\Delta z,n)$, it is necessary to fulfill the following condition:

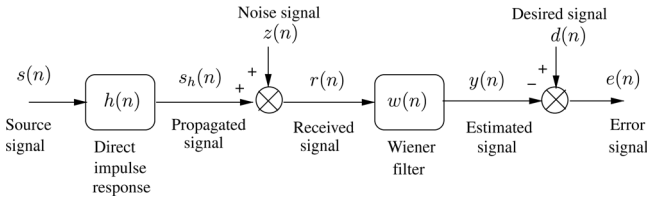

FIG. 7. Optimum filtering: The aim is to find the Wiener filter $w(n)$ which minimizes the mean square error $e(n)$ between the desired signal $d(n)$ and the estimated signal $y(n)$.

$$h^{-1}(k_x, k_y, \Delta z, n) * h(k_x, k_y, \Delta z, n) = \delta(n). \tag{26}$$

In order to ensure the causality of $h^{-1}(k_x, k_y, \Delta z, n)$, the right part of Eq. (26) must be replaced with $\delta(n-N)$. Optimum Wiener filtering may solve this problem.[2] Many applications in acoustics indeed successfully reach their goals by the use of a Wiener filter: Source deconvolution in exploration seismology,[25] in water environment,[26] binaural reproduction of stereo sound,[27–29] and active control of sound and vibration.[30] In these cases, the Wiener's problem of finding a filter in order to minimize the mean square error between the estimated signal $y(n)$ and the desired signal $d(n)$ is represented in a block diagram (see Fig. 7). The choice of the desired signal $d(n)$ provides a degree of freedom for the approach. When the desired signal $d(n)$ is the propagated signal $s_h(n)$, the aim of the Wiener filter $w(n)$ is to suppress the noise $z(n)$ from the received signal $r(n)$. This configuration can be used in standard NAH in the frequency-wavenumber domain before back-propagating the wavenumber spectrum for each frequency from the measurement plane to the source plane. The measurement noise is then attenuated by the Wiener filter in the wavenumber domain just before exponential amplification of the wavenumbers in the area corresponding to evanescent waves. In fact, this Wiener filter is a particularly case of the standard Tikhonov filter for which the regularization parameter is taken as the inverse of the signal-to-noise ratio. When the desired signal $d(n)$ is the source signal $s(n)$, the Wiener filter $w(n)$ solves an inverse problem: Inverting the direct impulse response $h(n)$. By considering an impulse sound source $s(n) = \delta(n)$ or its delayed version $s(n) = \delta(n-N)$ [with N as the number of samples of the impulse response $h(n)$] in order to have a causal inverse filter, the searched solution $h^{-1}(k_x, k_y, \Delta z, n)$ is obtained by minimizing the mean square error criterion

$$J(k_x, k_y, \Delta z) = \sum_{n=-\infty}^{+\infty} [\delta(n-N) - h(k_x, k_y, \Delta z, n) * h^{-1}(k_x, k_y, \Delta z, n)]^2. \tag{27}$$

The solution sought corresponds to the impulse response of a FIR filter with $h^{-1}(k_x, k_y, \Delta z, n) = 0$ for $n < 0$ and $n \geq N$.

Thus Eq. (27) yields

$$J(k_x, k_y, \Delta z) = \sum_{n=-\infty}^{+\infty} \left[\delta(n-N) - \sum_{m=0}^{N-1} h^{-1}(k_x, k_y, \Delta z, m) \times h(k_x, k_y, \Delta z, n-m) \right]^2. \tag{28}$$

The minimization of criterion $J(k_x, k_y, \Delta z)$ leads to the Wiener-Hopf equations[2] which can be written in the compact matrix form as

$$\mathbf{h^{-1}} = \mathbf{\Phi_h^{-1}} \mathbf{h^r}, \tag{29}$$

where $\mathbf{h^{-1}}$ is the vector of the solutions, $\mathbf{\Phi_h}$ the correlation matrix of the direct filter, and $\mathbf{h^r}$ the reverse vector of the direct filter [$\mathbf{h}(n) = \mathbf{h^r}(N-1-n)$, $n = 0, N-1$], which is derived from the cross-correlation between the direct filter and the desired signal (the Dirac delta function). Inverting the correlation matrix can be done using the regularization solution as

$$\mathbf{h^{-1}} = \left(\mathbf{\Phi_h^H \Phi_h} + \lambda \mathbf{I}\right)^{-1} \mathbf{\Phi_h^H h^r}, \tag{30}$$

with λ as the regularization parameter, $\mathbf{I}$ as the identity matrix, and $\mathbf{\Phi_h^H}$ as the transconjugate of matrix $\mathbf{\Phi_h}$. The inverse filter is causal, but the discrete time-dependent wavenumber spectrum $P(k_x, k_y, z_S, n)$, obtained on the source plane from Eq. (25), is delayed with a time delay equal to the number of samples N of the impulse response. Note that it does not prevent the method from continuously providing the time-dependent wavenumber spectrum on the source plane.

V. NUMERICAL RESULTS

A. Set-up

Three monopoles driven by nonstationary signals radiate from the source plane at the positions M_1 (0.3125, 0.375, 0 m), M_2 (0.75, 0.75, 0 m), and M_3 (0.25, 0.75, 0 m). Both monopoles M_1 and M_2 generate a signal with a linear frequency modulation in the band [200, 1800] Hz and a Gaussian amplitude modulation. Monopole M_3 radiates a Morlet wavelet according to the expression

$$s(t) = \cos(2\pi f_0 t) e^{-t^2/2}, \tag{31}$$

with $f_0 = 800$ Hz. A 17×17 microphone array is used for the simulation. It is located in the measurement plane $z = z_A = 0.1575$ m, as shown in Fig. 1. The step size in both x and y directions is $\Delta L = 0.0625$ m, providing an overall scan dimension of 1.0×1.0 m^2. For industrial applications the aim of real-time acoustic holography is of course to continuously reconstruct the time-dependent pressure field on the source plane. But here, another reconstructed plane is chosen to evaluate the accuracy of the method because of the singularity of the pressure of a monopole on the source plane. Time-dependent reference pressure field will be calculated on this plane from the sources. The back-propagation distance between the measurement plane and the reconstructed plane is $\Delta z = 0.1075$ m so that the reconstructed pressure is computed in the plane $z_R = 0.05$ m. The emitted signals are sampled at a frequency $f_e = 16\,000$ Hz providing 256 samples. This set-up is similar to that used in Ref. 14 for the study of forward propagation of time-evolving acoustic pressure.

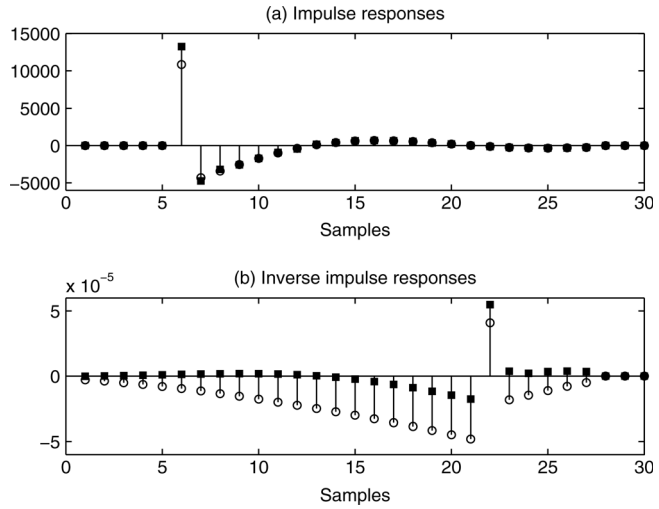

FIG. 8. Direct impulse responses $h(k_x, k_y, z_A - z_R, n)$ (a) and inverse impulse responses $h^{-1}(k_x, k_y, z_A - z_R, n)$ (b) truncated at 30 samples, obtained for one location of the wavenumber spectrum $k_x = 11.83\ \mathrm{rd\,m^{-1}}$ and $k_y = 11.83\ \mathrm{rd\,m^{-1}}$ with the direct (circular markers) and the Chebyshev (square markers) methods.

The goal of the current study is to provide the time-dependent pressure signal on a virtual grid which is the projection of the microphone array onto the reconstructed plane. It is easily done by using the two dimensional inverse spatial Fourier transform once the time-dependent wavenumber spectrum is computed on the reconstructed plane. The inverse spatial Fourier transform is the inverse operator of the discrete Fourier transform which was applied to the time-signals acquired by the microphone array to provide the instantaneous wavenumber spectrum. According to the sampling theorem in space domain, the maximal spatial frequency considered is $\pi/\Delta L\ \mathrm{rd\,m^{-1}}$ and the smallest spatial frequency which can be resolved is $2\pi\ \mathrm{rd\,m^{-1}}$. Thus the key-point is to obtain the back-propagated wavenumber spectrum on the plane $z = z_R$. It is based on the equation

$$P(k_x, k_y, z_R, t) = P(k_x, k_y, z_A, t) * h^{-1}(k_x, k_y, z_A - z_R, t). \tag{32}$$

Wiener optimum filtering is achieved to compute the inverse impulse response $h^{-1}(k_x, k_y, z_A - z_R, t)$ from different impulse responses $h(k_x, k_y, z_A - z_R, t)$ for each pair (k_x, k_y) of the time-wavenumber domain. The latter are built from the Chebyshev method (C), the numerical Kaiser method (N), the average method (A), the FD method, and the direct method (D) for which the impulse response is provided by directly sampling $g(\Omega_r, \tau, t)$ in Eq. (14) at $f_e = 16\,000$ Hz or $f_e = 64\,000$ Hz. The other approach denoted FI method, based on the inverse Fourier transform of $H^{-1}(\Omega_r, \tau, \omega)$ [see Eq. (23)], is also tested. Figure 8(a) shows two examples of direct impulse responses $h(k_x, k_y, z_A - z_R, n)$ obtained from the direct and the Chebyshev methods for a location ($k_x = 11.83\ \mathrm{rd\,m^{-1}}$, $k_y = 11.83\ \mathrm{rd\,m^{-1}}$) of the wavenumber spectrum. Figure 8(b) shows the corresponding inverse impulse responses $h^{-1}(k_x, k_y, z_A - z_R, n)$. The MATLAB language was used to implement the computation.

B. Indicators

Two time indicators T_1 and T_2 are used [see Eqs. (33) and (34)] to describe the results obtained objectively. They are based on the reconstructed signals $p(x, y, z_R, t)$ and on simulated signals $p_r(x, y, z_R, t)$, considered as reference signals directly propagated on the plane $z = z_R$. For the comparison based on the indicators, the time delay of the reconstructed signals, due to the inverse process of the impulse response, is compensated:

$$T_1 = \frac{\langle p_r(x, y, z_R, t) p(x, y, z_R, t) \rangle}{\sqrt{\langle p_r^2(x, y, z_R, t) \rangle \langle p^2(x, y, z_R, t) \rangle}}, \tag{33}$$

$$T_2 = \frac{\left| p_r^{\mathrm{rms}}(x, y, z_R) - p^{\mathrm{rms}}(x, y, z_R) \right|}{p_r^{rms}(x, y, z_R)}, \tag{34}$$

where $p_r^{\mathrm{rms}}(x, y, z_R)$ and $p^{\mathrm{rms}}(x, y, z_R)$ are the pressure root mean square values given by

$$p_r^{\mathrm{rms}}(x, y, z_R) = \sqrt{\langle p_r^2(x, y, z_R, t) \rangle}, \tag{35}$$

$$p^{\mathrm{rms}}(x, y, z_R) = \sqrt{\langle p^2(x, y, z_R, t) \rangle}. \tag{36}$$

$\langle\ \rangle$ is the time averaged value.

T_1, as a correlation coefficient, is sensitive to the similarity between the shapes of the signals and thus between their phase difference. T_2, defined as the relative difference between the root mean square values of the two signals, provides information on the magnitude accuracy of the reconstructed signals.

C. Results

Figure 9 highlights the time pressure signals $p(0.25, 0.75, 0.05\,\mathrm{m}, t)$ reconstructed in R_3 facing the monopole M_3 (see Fig. 1). The pressure signals are provided by convolving $P(k_x, k_y, z_A, t)$ the time-dependent wavenumber spectrum in the measurement plane $z = z_A$ over the inverse impulse responses resulting from Wiener optimum filtering of the impulse responses provided by the direct method for $f_e = 16\,000$ Hz [Fig. 9(a)], for $f_e = 64\,000$ Hz [Fig. 9(d)], the Chebyshev method [Fig. 9(b)], the average method [Fig. 9(c)], the numerical Kaiser method [Fig. 9(e)], and the FD method [Fig. 9(f)]. Through indicators T_1 and T_2, the reconstructed pressure signals are objectively compared to the reference pressure signals directly propagated to the plane $z = z_R$ by simulation. The values of indicators T_1 and T_2 for reconstructed time-signals in locations R_1, R_2, R_3, and R_4 (see Fig. 1) are reported in Table I. A good similarity with regard to magnitude gives T_2 values near 0. Phase accuracy gives T_1 in the neighborhood of 1. The reconstructed signal using the most evident method called FI method is not shown as the indicator values are very poor. This result confirms that NAH is an ill-posed problem which must be solved with great care. It is well known that in NAH filtering in the wavenumber domain is required before reconstruction. The same requirements are needed when using RT-NAH on

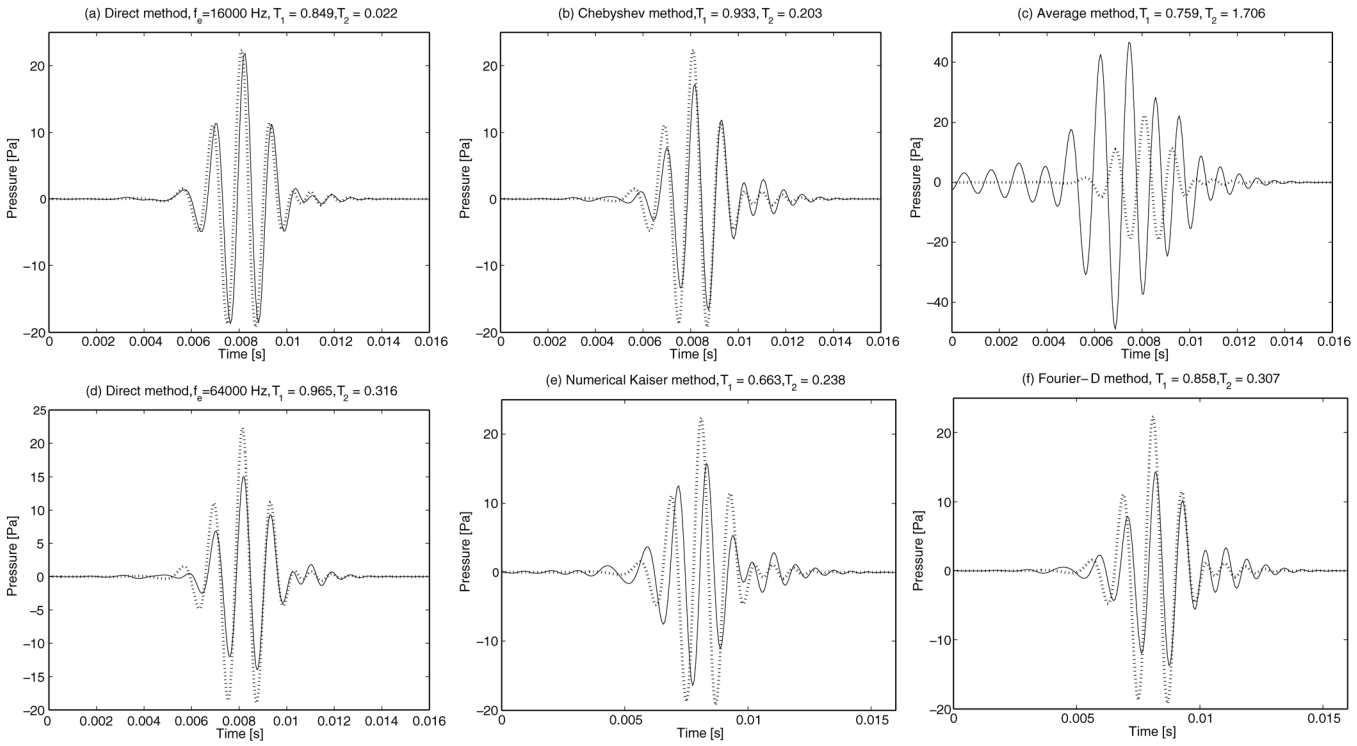

FIG. 9. Reconstructed time-signals (solid line) versus reference signals (dotted line) in the time-space domain in location R_3 (cf. Fig. 1) for different impulse response inversions computed by five methods [direct (a) and (d), Chebyshev (b), average (c), numerical Kaiser (e), Fourier-D (f)]. The indicators T_1 [Eq. (33)] and T_2 [Eq. (34)] are given on top of each graph.

nonstationary sources but in time-wavenumber domain. It is then necessary to filter the analytic inverse transfer function $H^{-1}(\Omega_r,\tau,\omega)$ by means of a Tikhonov filter $W_T(\Omega_r,\tau,\lambda,\omega)$ for instance, as proposed in Ref. 24, before operating the inverse Fourier transform of $H^{-1}_{\text{regul}}(\Omega_r,\tau,\omega)$,

$$H^{-1}_{\text{regul}}(\Omega_r,\tau,\omega)=H^{-1}(\Omega_r,\tau,\omega)W_T(\Omega_r,\tau,\lambda,\omega), \tag{37}$$

TABLE I. Indicators T_1 and T_2 [see Eqs. (33) and (34)] computed from reference signals and pressure signals backpropagated to the plane $z=z_R$ in locations R_1, R_2, R_3, and R_4 (see Fig. 1) using the inverse impulse responses obtained by the direct method [(D_1) with f_e = 16 000 Hz, (D_2) with f_e = 64 000 Hz], the average method (A), the Chebyshev method (C), the numerical Kaiser method (N), the FD method, and the FI method.

	D_1	D_2	A	C	N	FD	FI
				R_1			
T_1	0.780	0.913	0.617	0.888	0.654	0.831	0.884
T_2	0.030	0.249	1.523	0.124	0.179	0.160	8.616
				R_2			
T_1	0.756	0.921	0.758	0.900	0.636	0.868	0.888
T_2	0.014	0.135	0.394	0.005	0.292	0.162	9.749
				R_3			
T_1	0.849	0.965	0.759	0.933	0.663	0.858	0.967
T_2	0.022	0.316	1.706	0.203	0.238	0.307	6.205
				R_4			
T_1	0.855	0.993	0.590	0.943	0.843	0.833	0.602
T_2	0.086	0.114	7.478	0.119	1.212	0.164	16.305

with

$$W_T(\Omega_r,\tau,\lambda,\omega)=\begin{cases}\dfrac{1}{1+\lambda} & \text{for } \omega\geq\Omega_r,\\[2ex] \dfrac{1}{1+\lambda e^{2\tau\sqrt{\Omega_r^2-\omega^2}}} & \text{for } \omega<\Omega_r.\end{cases} \tag{38}$$

The most accurate reconstructed signal is obtained from the direct method when the signal is oversampled. The Chebyshev and the FD method give also interesting results with regard to the phase (T_1 indicator). It is clear that the average method and the numerical Kaiser method are not suitable for the inversion based on the optimum filtering approach used in the study. The same conclusions can be drawn from the examination of spatial maps given indicators T_1 and T_2 in the whole space. Figure 10 highlights some of these maps obtained by the direct method with two sampling frequencies f_e = 16 000 Hz [Fig. 10(a) for T_1, Fig. 10(b) for T_2], and f_e = 64 000 Hz [Fig. 10(e) for T_1, Fig. 10(f) for T_2], and the Chebyshev method [Fig. 10(c) for T_1, Fig. 10(d) for T_2]. The contour line value used for indicator T_1 is 0.95 in Figs. 10(a), 10(c), and 10(e). The gray area in Figs. 10(b), 10(d), and 10(e) correspond to T_2 values within the interval [0, 0.1]. This area is larger for the direct method with a sampling frequency f_e = 64 000 Hz. The locations facing the monopole sources do not give the best results in terms of phase similarity [see Figs. 10(a), 10(c), and 10(e)]. The use of the Chebyshev method [Fig. 10(c)] enhances this point in comparison to the direct method [Fig. 10(a)] experimented with the same sampling frequency f_e = 16 000 Hz. The error is also higher near the edges of the scanned area, but this problem is inherent with the field truncation by the hologram

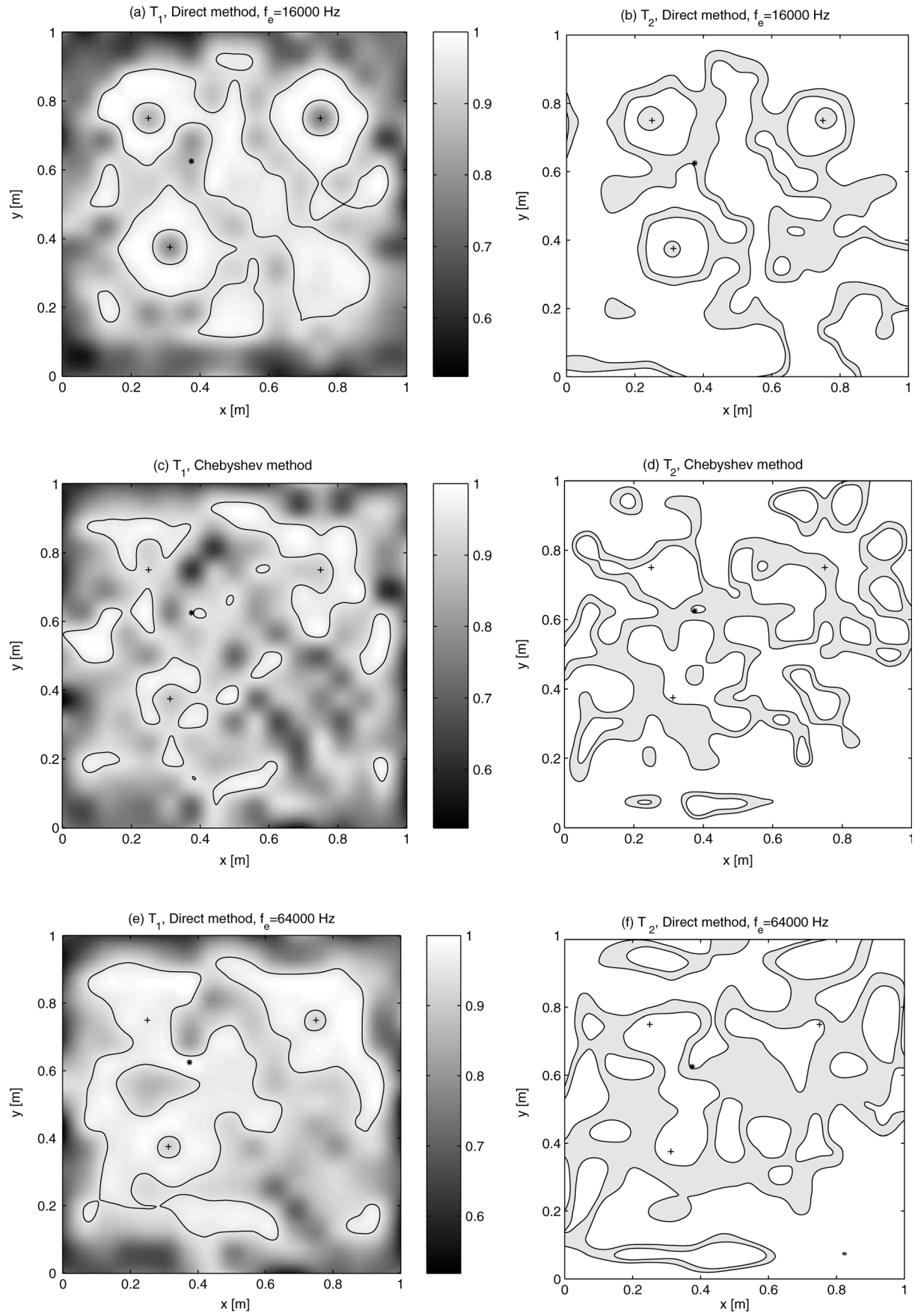

FIG. 10. Spatial maps for indicator T_1 and T_2 to, respectively, assess the phase and the amplitude similarities between the reference signals and the back-propagated signals using the direct method with two sampling frequency $f_e = 16\,000$ Hz (a), (b), $f_e = 64\,000$ Hz (e), (f), and the Chebyshev method (c), (d). The locations of $R_1(+)$, $R_2(+)$, $R_3(+)$, and $R_4(*)$ are marked. The contour line for indicator T_1 is set at the value 0.95 in (a), (c), and (e). For the (b), (d), and (f) graphs, the areas in gray correspond to values of T_2 within the interval $[0, 0.1]$.

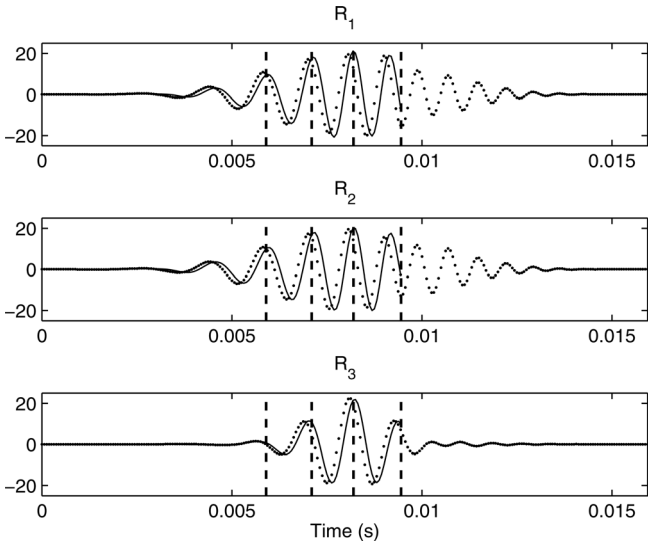

FIG. 11. Reconstructed time-signal on the plane $z_R = 0.05$ m using the direct method with $f_e = 16\,000$ Hz in three locations facing the monopoles. The reference signals are drawn using a dotted line. Four time instances $t_1 = 5.87$ ms, $t_2 = 7.12$ ms, $t_3 = 8.19$ ms, and $t_4 = 9.44$ ms are marked using vertical dashed lines. The spatial acoustic fields corresponding to these time instances are shown in Fig. 12.

and can be reduced by selective spatial filtering using wavelets.[31]

Upsampling of the impulse response before inverse Wiener filtering enhances the reconstruction error, particularly with regard to the signal phase. This parameter seems to be more relevant than processing the impulse responses. This result differs from those obtained on forward reconstructed time-dependent acoustic fields.[14] In that study, processing the impulse response appeared as a necessary condition to reach a correct reconstruction error while working with a higher sampling rate was not sufficient. In the case of RT-NAH, the contribution of the processing techniques on the impulse response in the time-wavenumber domain has not been yet demonstrated. The numerical Kaiser method which led to the best forward reconstruction error is not appropriate for solving the inverse problem when Wiener optimum filtering is used for inverting the impulse response. One assumption for that is the ill-posed nature of NAH. It is probably necessary in future works to enhance the inverting process of the correlation matrix in Eq. (29) as mentioned in Eq. (30). In addition, using regularization techniques for inverting the impulse response for recovering time-dependent acoustic fields seems promising.[32] And in this case, the reconstruction error seems sensitive to the method used for processing the impulse response.

D. Interest of the method

Figures 11 and 12 are intended to show the interest of RT-NAH. Indeed, the technique continuously provides information on how the acoustic sources radiate. Time-signals from spatial locations or images of the field radiated by sources are provided at any time: Each new time sample on the microphone array gives a new time sample on the reconstruction plane. It is different from time domain holography for which the pressure time-signals are reconstructed by data blocks. However, the aim of both methods is to reconstruct time-signals on the source plane. Let us observe the time-signals in Fig. 11. They have been reconstructed by RT-NAH using the direct method with $f_e = 16\,000$ Hz at three locations facing the sources M_1, M_2, and M_3. The reference signals are drawn in dotted line showing an error in the phase of the reconstruction. But it is not the point here as we want to focus on the time evolution of the acoustic field radiated by the sources. Four time instances $t_1 = 5.87$ ms, $t_2 = 7.12$ ms, $t_3 = 8.19$ ms, and $t_4 = 9.44$ ms are arbitrarily chosen (see the vertical dashed lines in Fig. 11). The spatial fields corresponding to these time instances are shown in Fig. 12. At time t_1 (a), as it can be checked in Fig. 11, the acoustic field is dominated by the acoustic signals radiated by sources M_1 and M_2. At time t_2 (b), the level of radiation from the two previous sources is getting higher and the effect of the source M_3 is visible. At time t_3 (c), the acoustic field is composed of three sources which radiate highly and similarly. At time t_4 (d), only the source M_3 radiates with a low level. Thus RT-NAH provides a means of highlighting sound fluctuations both in time and space.

VI. CONCLUSION

The method called RT-NAH has the advantage to continuously reconstruct time acoustic signals on the source plane from measurements done in the near-field using a microphone array. The specificity of the method is that it operates in the time-wavenumber domain with the means of a convolution product between the time-dependent wavenumber spectrum recorded by the array and an inverse impulse response. Accordingly, the sound fields studied by this technique do not require to be radiated during a short time period as for time domain holography. In addition, the ability to provide time-signals on the source plane as if the sensors were embedded into the acoustic sources is promising. The reconstructed signals indeed can be post-processed in order to diagnose the behavior of any system making noise. For instance, a time-frequency analysis of the reconstructed signals would provide their time-evolving frequency content and then the time-evolving spatial pressure field for any frequency band chosen *a posteriori*. It is also an advantage over the transient method for which the frequency band of interest is chosen *a priori* at the beginning of the analysis. It is also possible to rebuild all other instantaneous acoustic quantities (velocity, sound intensity, …) or instantaneous physical quantities in a mechanical structure (strain, stress, power flow) whose vibrational field is identified on the reconstruction plane.

The heart of the method was shown to be inverting the impulse response. Upsampling the analytic direct impulse response or low-pass filtering it with a Chebyshev filter before inversion using Wiener optimum filtering gave interesting results in a simulated case involving three monopole sources driven by nonstationary signals. However, it appeared that improvement of the technique could be reached by reconsidering the inversion process with regularization approaches.

For RT-NAH experimentations, it is important to notice that each microphone of the array must record the acoustic

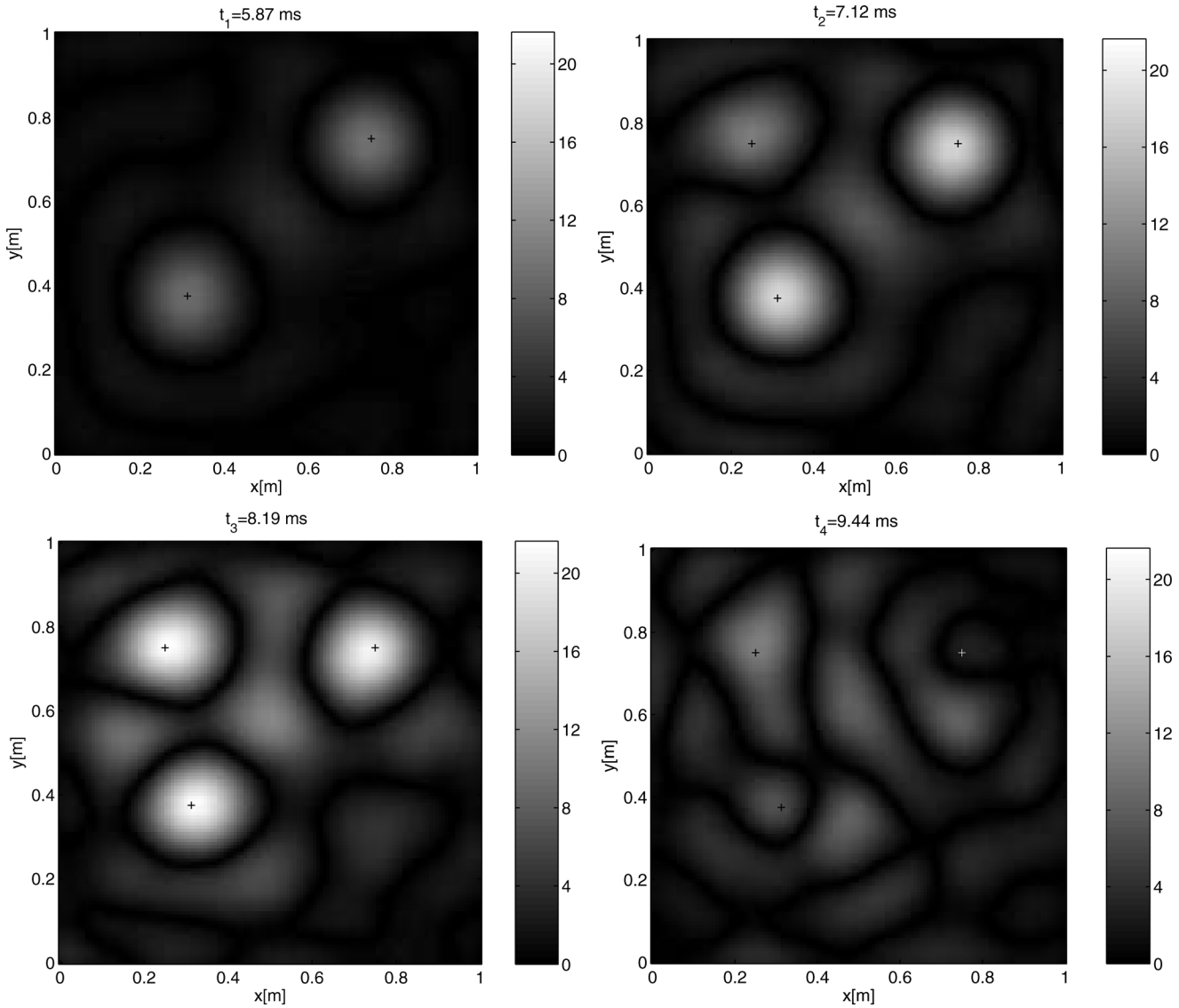

FIG. 12. Spatial pressure fields reconstructed by RT-NAH on the plane $z_R = 0.05$ m using the direct method with $f_e = 16\,000$ Hz at different time instances $t_1 = 5.87$ ms (a), $t_2 = 7.12$ ms (b), $t_3 = 8.19$ ms (c), and $t_4 = 9.44$ ms (d). The time instances are defined in Fig. 11. The acoustic field is radiated by the three sources defined in the study. The points facing the monopoles are marked (+).

field at the same time, which often requires hundreds of microphones and acquisition channels except if the sound radiation is repeatable.

[1]E. G. Williams, *Fourier Acoustics: Sound Radiation and Nearfield Acoustical Holography* (Academic Press, New York, 1999), pp. 1–306.
[2]S. Haykin, *Adaptive Filter Theory*, 3rd ed. (Prentice Hall, Englewood Cliffs, NJ, 1996), pp. 1–989.
[3]M. R. Bai, "Acoustical source characterization by using recursive Wiener filtering," J. Acoust. Soc. Am. **97**(5), Pt. 1, 2657–2663 (1995).
[4]J. F. Li, J.-C. Pascal, and C. Carles, "A new k-space optimal filter for acoustic holography," in *Proceedings of the 3rd International Congress on Air and Structure Borne Sound and Vibration*, Montreal, Canada (June, 1994), pp. 1059–1066.
[5]E. G. Williams, "Regularization methods for near-field acoustical holography," J. Acoust. Soc. Am. **110**(4), 1976–1988 (2001).
[6]J. Hald, "Time domain acoustical holography," *in Proceedings of Inter-Noise 1995*, Newport Beach, USA (July, 1995), pp. 1349–1354.
[7]J. Hald, *Non Stationary STSF* (Brüel & Kjaer Technical Review, Naerum, Denmark, 2000), pp. 1–36.
[8]J. Hald, "Time domain acoustical holography and its applications," Sound Vib. **35**, 16–25 (2001).
[9]F. Deblauwe, J. Leuridan, J. L. Chauray, and B. Béguet, "Acoustic holography in transient conditions," in *Proceedings of the Sixth International Congress on Sound and Vibration*, Copenhagen, Denmark (July, 1999), pp. 899–906.
[10]S. F. Wu, H. Lu, and M. S. Bajwa, "Reconstruction of transient acoustic radiation from a sphere," J. Acoust. Soc. Am. **117**(4), 2065–2077 (2005).
[11]M. R. Bai and J. H. Lin, "Source identification system based on the time-domain nearfield equivalence source imaging: Fundamental theory and implementation," J. Sound. Vib. **307**, 202–225 (2007).
[12]P. A. Nelson and S.H. Yoon, "Estimation of acoustic sources strength by inverse methods: Part I, conditioning of the inverse problem," J. Sound. Vib. **233**(4), 643–668 (2000).
[13]M. Forbes, S. Letcher, and P. Stepanishen, "A wave vector, time-domain method of forward projecting time-dependent pressure fields," J. Acoust. Soc. Am. **90**(5), 2782–2792 (1991).
[14]V. Grulier, S. Paillasseur, J.-H. Thomas, J.-C. Pascal, and J.-C. Le Roux, "Forward propagation of time evolving acoustic pressure: Formulation and investigation of the impulse response in time-wavenumber domain," J. Acoust. Soc. Am. **126**(5), 2367–2378 (2009).
[15]J. Hald, *STSF-A Unique Technique for Scan-Based Near-Field Acoustic Holography Without Restrictions on Coherence* (Brüel & Kjaer Technical Review, Naerum, Denmark, 1989), pp. 1–50.
[16]J.-F. Li, J.-C. Pascal, and C. Carles, "Acoustic energy fields of partially coherent sources," J. Acoust. Soc. Am. **103**(2), 962–972 (1998).

[17]M. Lee and J. S. Bolton, "Scan-based near-field acoustical holography and partial field decomposition in the presence of noise and source level variation," J. Acoust. Soc. Am **119**(1), 382–393 (2006).
[18]H.-S. Kwon and Y.-H. Kim, "Moving frame technique for planar acoustic holography," J. Acoust. Soc. Am. **103**(4), 1734–1741 (1998).
[19]J.-F. Blais and A. Ross, "Backward propagation of sound fields radiated by impacted plates using a transient acoustical holography approach," in *Proceedings of Inter-Noise 2009*, Ottawa, Canada (August, 2009), pp. 1–916.
[20]P. C. Hansen, *Rank-Deficient and Discrete Ill-Posed Problems* (SIAM, Philadelphia, 1998), pp. 1–247.
[21]O. de la Rochefoucauld, M. Melon, and A. Garcia, "Time domain holography: Forward projection of simulated and measured sound pressure fields," J. Acoust. Soc. Am. **116**(2), 142–153 (2004).
[22]J.-F. Blais and A. Ross, "Forward projection of transient sound pressure fields radiated by impacted plates using numerical Laplace transform," J. Acoust. Soc. Am. **125**(5), 3120–3128 (2009).
[23]S. Mallat, *A Wavelet Tour of Signal Processing*, 2nd ed. (Academic Press, London, 1998), pp. 1–637.
[24]V. Grulier, "Propagation directe et inverse dans l'espace temps-nombre d'onde: Application à une méthode d'holographie acoustique de champ proche pour les sources non stationnaires (Direct and inverse propagation in the time-wavenumber domain: Application to a nearfield acoustic holography method for non stationary sources)," Ph.D. dissertation, Université du Maine, Le Mans, France, 2005, pp. 1–121.
[25]C. Chang and Q.-H. Liu, "Inversion of source-time functions using borehole array sonic waveforms," J. Acoust. Soc. Am. **103**(6), 3163–3168 (1998).
[26]B. S. Cazzolato, P. Nelson, P. Joseph, and R. J. Brind, "Numerical simulation of optimal deconvolution in a shallow-water environment," J. Acoust. Soc. Am. **110**(1), 170–185 (2001).
[27]S.-M. Kim and S. Wang, "A Wiener filter approach to the binaural reproduction of stereo sound," J. Acoust. Soc. Am. **114**(6), 3179–3188 (2003).
[28]S.-M. Kim and W. Choi, "On the externalization of virtual sound images in headphone reproduction: A Wiener filter approach," J. Acoust. Soc. Am. **117**(6), 3657–3665 (2005).
[29]O. Kirkeby, P. A. Nelson, H. Hamada, and F. Orduna-Bustamante, "Fast deconvolution of multichannel systems using regularization," IEEE Trans. Speech Audio Process. **6**(2), 189–194 (1998).
[30]M. J. Brennan and S.-M. Kim, "Feedforward and feedback control of sound and vibration—A Wiener filter approach," J. Sound Vib. **110**(1), 281–296 (2001).
[31]J.-H. Thomas and J.-C. Pascal, "Wavelet preprocessing for listening truncation effects in nearfield acoustical holography," J. Acoust. Soc. Am. **118**(2), 851–860 (2005).
[32]S. Paillasseur, J.-H. Thomas, and J.-C. Pascal, "Regularization method applied to the determination of the inverse filter of Real-Time Nearfield Acoustic Holography," in *Proceedings of Inter-Noise 2009*, Ottawa, Canada (August, 2009).